Metal Tolerance Protein 8 Mediates Manganese Homeostasis and Iron Reallocation during Seed Development and Germination[1][OPEN]

Seckin Eroglu,[a,b,2] Ricardo F. H. Giehl,[a,2] Bastian Meier,[c] Michiko Takahashi,[d] Yasuko Terada,[e] Konstantin Ignatyev,[f] Elisa Andresen,[g] Hendrik Küpper,[g] Edgar Peiter,[c] and Nicolaus von Wirén[a,3]

[a]Molecular Plant Nutrition, Leibniz-Institute for Plant Genetics and Crop Plant Research, D-06466 Gatersleben, Germany
[b]Department of Genetics and Bioengineering, Izmir University of Economics, 35330 Izmir, Turkey
[c]Plant Nutrition Laboratory, Institute of Agricultural and Nutritional Sciences, Martin Luther University Halle-Wittenberg, D-06099 Halle (Saale), Germany
[d]Laboratory of Plant Nutrition, Department of Plant Science, Faculty of Agriculture, Utsunomiya University, 321-8505 Utsunomiya, Japan
[e]Spring-8, Japan Synchrotron Radiation Research Institute, 679-5198 Japan
[f]Diamond Light Source, Harwell Science and Innovation Campus, OX11 0DE Didcot, United Kingdom
[g]Biology Centre of the Czech Academy of Sciences, Institute of Plant Molecular Biology, Department of Plant Biophysics and Biochemistry, CZ-37005 České Budějovice, Czech Republic

ORCID IDs: 0000-0002-9494-7080 (S.E.); 0000-0003-1006-3163 (R.F.H.G.); 0000-0003-3270-5825 (B.M.); 0000-0002-8937-5655 (K.I.); 0000-0002-7201-2508 (E.A.); 0000-0003-0712-7023 (H.K.); 0000-0002-9104-3238 (E.P.); 0000-0002-4966-425X (N.v.W.).

Metal accumulation in seeds is a prerequisite for germination and establishment of plants but also for micronutrient delivery to humans. To investigate metal transport processes and their interactions in seeds, we focused on METAL TOLERANCE PROTEIN8 (MTP8), a tonoplast transporter of the manganese (Mn) subclade of cation diffusion facilitators, which in Arabidopsis (*Arabidopsis thaliana*) is expressed in embryos of seeds. The x-ray fluorescence imaging showed that expression of MTP8 was responsible for Mn localization in subepidermal cells on the abaxial side of the cotyledons and in cortical cells of the hypocotyl. Accordingly, under low Mn availability, MTP8 increased seed stores of Mn, required for efficient seed germination. In mutant embryos lacking expression of *VACUOLAR IRON TRANSPORTER1* (*VIT1*), MTP8 built up iron (Fe) hotspots in *MTP8*-expressing cells types, suggesting that MTP8 transports Fe in addition to Mn. In *mtp8 vit1* double mutant seeds, Mn and Fe were distributed in all cell types of the embryo. An Fe transport function of MTP8 was confirmed by its ability to complement Fe hypersensitivity of a yeast mutant defective in vacuolar Fe transport. Imbibing *mtp8-1* mutant seeds in the presence of Mn or subjecting seeds to wet-dry cycles showed that MTP8 conferred Mn tolerance. During germination, MTP8 promoted reallocation of Fe from the vasculature. These results indicate that cell type-specific accumulation of Mn and Fe in seeds depends on MTP8 and that this transporter plays an important role in the generation of seed metal stores as well as for metal homeostasis and germination efficiency under challenging environmental conditions.

The formation of viable seeds in flowering plants requires a continuous delivery of mineral elements from the maternal tissue into the developing seed (Thorne, 1985). As shown by the movement of green fluorescent proteins, entry of assimilates and probably also of mineral elements from the outer integument, which represents a symplastic extension of the maternal vascular tissue, to the endosperm and further to the embryo involves the passage of apoplastic borders (Stadler et al., 2005). These are located between the outer integument and the endosperm, and between the endosperm and the epidermis of the embryo (Tegeder, 2014). From the heart stage onwards, the embryo forms a single symplastic domain and depends on substrate delivery from the endosperm. In mature embryos, the hypocotyl and the root vasculature form an independent symplastic domain, and individual cells along the leaf vascular bundles show poor symplastic connectivity to their adjacent cells (Stadler et al., 2005). The formation of independent symplastic domains during embryo development implies that the distribution of mineral elements between different cell types becomes more restricted.

Metals reach the embryo via different routes and at different developmental stages. In Arabidopsis (*Arabidopsis thaliana*), manganese (Mn) enters the embryo of developing seeds at the bent cotyledon stage, after Mn has been released from its transient store in the chalazal endosperm (Otegui et al., 2002). In contrast, Perls'/DAB staining of isolated embryos showed that iron (Fe) starts accumulating in the embryo already from the walking stick stage on (Roschzttardtz et al., 2009).

During these early stages of embryo maturation, Fe is mostly localized in chloroplasts where it supports photosynthetic activity (Divol et al., 2013). As photosynthesis in embryos ceases during postmaturation, large amounts of Fe are released from the thylakoids into the cytosol for subsequent loading into vacuoles. In the following, a major part of the Fe and Mn adopts a particular and highly defined cell type-specific distribution in postmature embryos (Kim et al., 2006; Punshon et al., 2012; 2013). A large fraction of embryonic Fe is then stored in endodermal cells that surround the vasculature in the hypocotyl or radicle axis and in cotyledons (Kim et al., 2006; Schnell and Ramos et al., 2013; Roschzttardtz et al., 2009). By contrast, Mn is mainly concentrated in cortical cells of the hypocotyl and radicle and in subepidermal cells of the abaxial side of cotyledons (Kim et al., 2006). Up to 30% of the total Mn in dry seeds can be located within these areas (Schnell Ramos et al., 2013). At the subcellular level, large amounts of Fe and Mn precipitate as phytate crystals and are found in the form of globoids in protein storage vacuoles (Bruch et al., 2015; Donner et al., 2012; Hunter et al., 2007; Lanquar et al., 2005; Mary et al., 2015; Otegui et al., 2002; Raboy, 2003; Roschzttardtz et al., 2009). Fe loading into endodermal vacuoles is mediated by the VACUOLAR IRON TRANSPORTER1 (VIT1; Kim et al., 2006). In *vit1* loss-of-function mutants of Arabidopsis, Fe localization around the vasculature is completely disrupted (Kim et al., 2006; Roschzttardtz et al., 2009), suggesting that VIT1 is the major transporter responsible for the cell type-specific localization of Fe in mature embryos. Intriguingly, in *vit1* embryos, Fe colocalizes with Mn in the cortical cells of the hypocotyl and radicle, and in the subepidermal cells of the abaxial side of cotyledons (Kim et al., 2006; Schnell Ramos et al., 2013). Noteworthy, also in this alternative accumulation site, Fe is still mainly confined to vacuoles (Roschzttardtz et al., 2009), indicating that in the absence of VIT1, Fe and Mn may share the same pathway for vacuolar loading. However, up to now the molecular identity of the transporter(s) responsible for cell-specific Mn localization in embryos has remained elusive.

During seed germination, nutrient stores are remobilized to sustain the demand of the developing seedling as long as efficient nutrient uptake systems in roots are not yet in place. The early phase of seed germination starts with imbibition, when water is rapidly taken up and metabolic activities that were suspended during seed desiccation become reactivated (Weitbrecht et al., 2011). Already from the first day of germination, Fe is released from vacuolar stores via the tonoplast-localized transporters NATURAL RESISTANCE ASSOCIATED MACROPHAGE PROTEIN3 (NRAMP3) and NRAMP4 (Lanquar et al., 2005). Interestingly, NRAMP3 and NRAMP4 remobilize specifically the Fe pool that has been formed by VIT1 in endodermal cells during embryo development (Roschzttardtz et al., 2009; Mary et al., 2015). This NRAMP3- and NRAMP4-dependent remobilization of the VIT1-formed Fe pool is critical for the successful establishment of the seedling, especially under Fe-deficient conditions (Kim et al., 2006; Lanquar et al., 2005). Thus, it has been suggested that VIT1, NRAMP3, and NRAMP4 represent a functional module that operates in endodermal cells surrounding the vasculature of embryos and is responsible for the formation of Fe stores during embryo development and their efficient remobilization during seed germination (Mary et al., 2015). However, it is noteworthy that the Fe stored in cortical cells of hypocotyl/radicle and in subepidermal cells located in the abaxial side of cotyledons in *vit1* mutants can be remobilized during germination also in the absence of functional NRAMP3 and NRAMP4 transporters (Mary et al., 2015). Thus, these cells may harbor another as-yet-unknown vacuolar "influx-efflux transporter module" that is not only responsible for Mn accumulation but may also use Fe as substrate.

In contrast to NRAMPs, which can permeate a broad range of different metals (Curie et al., 2000; Thomine et al., 2000), the Mn subgroup of CATION DIFFUSION FACILITATOR/METAL TOLERANCE PROTEINS (CDF/MTPs) has been described as rather specific for Mn transport (Migeon et al., 2010; Montanini et al., 2007; Peiter et al., 2007). Recently, we characterized MTP8 as a tonoplast Mn transporter in Arabidopsis roots that is part of the Fe-deficiency response, preventing plants from Mn toxicity by protecting the Fe acquisition machinery (Eroglu et al., 2016). Publicly available microarray data indicated that *MTP8* is also expressed in seeds and up-regulated as seeds develop inside siliques. By assessing metal distribution in wild-type and *mtp8* mutant seeds with the help of x-ray fluorescence microscopy (μXRF), we show here that MTP8 is responsible for defining Mn hotspots in the hypocotyl and cotyledons during seed development as well as for reallocating Fe during germination or when VIT1 is not functional. Our

[1] This work was supported by the Bundesministerium für Forschung und Bildung, Bonn (FKZ 0315458B to N.v.W), the Deutsche Forschungsgemeinschaft (DFG, PE1500/3-1 to E.P.), the Ministry of Education of the Czech Republic with co-financing from the European Union (KOROLID, CZ.02.1.01/0.0/0.0/15_003/0000336 to H.K.), the Czech Academy of Sciences (RVO 60077344 to H.K.), and the Scientific and Technological Council of Turkey, Ankara (fellowship to S.E. ,BIDEB-2232, 116C059). We acknowledge Diamond Light Source for time on Beamline i18 under Proposals SP11892 and SP13852.

[2] These authors contributed equally to the article.

[3] Address correspondence to vonwiren@ipk-gatersleben.de.

The author responsible for distribution of materials integral to the findings presented in this article in accordance with the policy described in the Instructions for Authors (www.plantphysiol.org) is: Nicolaus von Wirén (vonwiren@ipk-gatersleben.de).

S.E., R.F.H.G., and B.M. performed most experiments; H.K., K.I., E.A., and E.P. performed μXRF tomography of intact seeds; M.T. and Y.T. performed 2D-μXRF imaging of seed sections; E.P. and N.v.W. designed the experiments and analyzed the data; E.P. and N.v.W. conceived the project and wrote the article with contributions of all the authors.

[OPEN] Articles can be viewed without a subscription.

www.plantphysiol.org/cgi/doi/10.1104/pp.16.01646

results further reveal a role for MTP8 in building up Mn stores that support seed germination after plant growth under Mn deficiency or prevent seeds from Mn overflow during imbibition. Thereby, this study identifies MTP8 as a missing link in the generation of vacuolar Mn and Fe stores and describes its (eco-) physiological role during the early phases of germination.

RESULTS

MTP8 Expression in Developing Seeds

In a search for metal transporters involved in seed loading and homeostasis of Mn, we recognized that the *MTP8* is highly expressed in sepals, stamens, and seeds (Supplemental Fig. 1A). Previously, we showed that in Fe-sufficient Arabidopsis plants *MTP8* is weakly expressed in most vegetative organs but strongly inducible in outer root cells, where it is under strict control of the Fe deficiency-induced transcriptional regulator FIT (Eroglu et al., 2016). To validate the in silico seed expression data, we assessed promoter activity of *MTP8* in embryos of developing seeds employing *promoterMTP8:GUS* lines. Histochemical analyses revealed that *MTP8* promoter activity in the seed was absent during the early developmental stages, while it increased strongly during the green cotyledon stage and at maturity (Fig. 1). In maturing embryos, *MTP8* promoter activity was most prominent in the hypocotyl and cotyledons, but not in the apical part of the hypocotyl and root. Notably, promoter activity and expression was confined to the embryo and not detected in the seed coat or endosperm (Fig. 1; Supplemental Fig. 1B). To compare the spatial and temporal expression pattern of *MTP8* to that of the tonoplast Fe transporter *VIT1*, *promoterVIT1:GUS* lines were assessed in parallel. In contrast to *MTP8*, promoter activity of *VIT1* was detected throughout seed development and rather pronounced in provascular strands of the embryo (Fig. 1). These observations indicated that the promoter activity of *MTP8* differed from that of *VIT1* temporally, as *MTP8* promoter activity set in when the embryo was fully developed and approached maturity and, spatially, as it expanded over a larger tissue area than that of *VIT1*.

Metal Distribution in Mature *mtp8* Mutant Seeds as Determined by μXRF

Since *MTP8* expression is induced in maturing embryos (Fig. 1), we assessed whether the loss of MTP8 alters the distribution of Mn and other metals in mature seeds. Thus, dry seeds of wild-type and two independent *mtp8* mutant lines (Eroglu et al., 2016) were analyzed by μXRF for metal localization. In agreement with previous reports (Kim et al., 2006; Schnell Ramos et al., 2013; Mary et al., 2015), wild-type seeds enriched Fe strongly in the provascular tissue of the hypocotyl and in the three provascular strands of each of the cotyledons, whereas Mn was highly confined to the abaxial side of the cotyledons and in cortical cells of the hypocotyl (Fig. 2). Importantly, the characteristic pattern of Fe distribution was not affected by the loss of MTP8. However, in seeds of both *mtp8* mutants, Mn lost its predominant localization in the subepidermal cells of the abaxial side of the cotyledons and hypocotyl. Instead, Mn accumulated in the provascular tissue and adopted specifically the localization pattern of Fe (Fig. 2). In contrast, Zn was more homogeneously distributed throughout the embryo (Fig. 2). The distribution pattern of this metal was not specifically altered in *mtp8* seeds. These results suggested that MTP8 confers cell type-specific accumulation of Mn in cotyledons and that in the absence of MTP8 Mn transport processes largely overlap with those of Fe.

Unexpectedly, the Mn signal in the two *mtp8* mutants was weaker than in Col-0 (Fig. 2, note the different

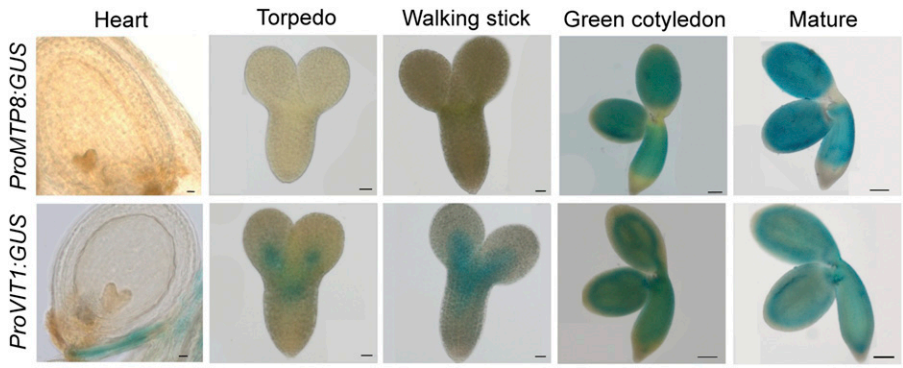

Figure 1. *MTP8* and *VIT1* promoter activities in developing embryos. *PromoterMTP8:GUS* and *PromoterVIT1:GUS* lines were grown on soil, and seeds were harvested from developing siliques to obtain seeds with embryos at the indicated developmental stages. Isolated embryos were incubated in GUS solution overnight for heart, torpedo, and walking stick stages, or for 2 h for green cotyledon and mature stages. Scale bars represent 100 μm for heart, torpedo, and walking stick stages and 20 μm for green cotyledon and mature stages.

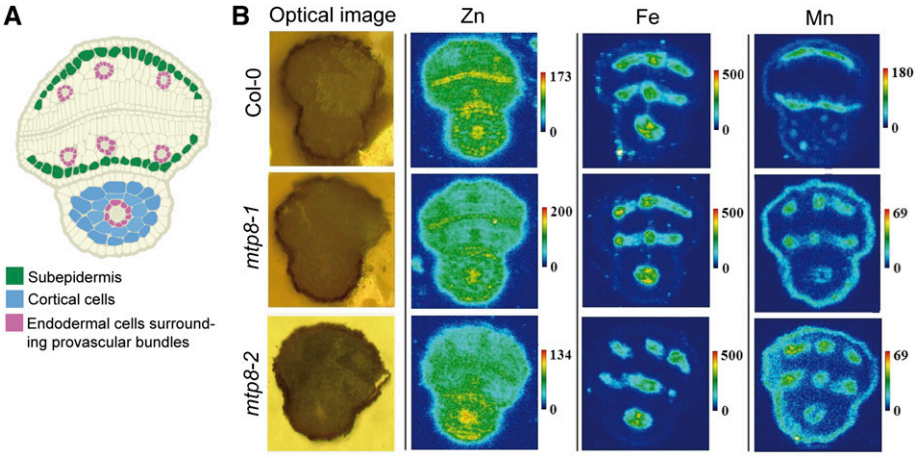

Figure 2. μXRF imaging of seed sections. A, Schematic representation of a cross section of a mature Arabidopsis seed highlighting cell types relevant for metal localization in embryos. B, Transversal images of light microscopy or x-ray fluorescence show relative abundances of individual metals. Dry seeds of wild-type, *mtp8-1*, and *mtp8-2* mutant plants were imbibed in water for 3 h, and metal localization in seeds was analyzed on cross sections. Seeds were obtained from plants propagated under the same conditions. At least three different seeds from each line were analyzed and representative images are shown.

scaling). We considered that this may be due to the μXRF imaging approach on sections, which we used at the Spring8 facility. We therefore undertook an independent study on metal localization in intact seeds by synchrotron μXRF tomography at the Diamond Light Source facility, in which we included seeds from *vit1-1* single and *mtp8 vit1* double mutant lines. Due to higher resolution and tomographic recording, this analysis prevented sectioning artifacts, allowed more refined quantification, and yielded similar signal intensities for Mn in wild-type and *mtp8-1* seeds. This analysis confirmed Mn accumulation in subepidermal cells of the two cotyledons and in cortical cells of the hypocotyl of wild-type and *vit1-1* seeds, while Mn localized to the provascular tissue in *mtp8-1* seeds (Fig. 3). In *mtp8 vit1* seeds, however, cell type-specific localization of Mn got lost. Interestingly, this observation also held true for Fe, which now appeared evenly distributed within the embryo tissue. These images indicated not only that MTP8 was responsible for the subepidermal localization of Mn, and in the absence of VIT1 also of Fe, but also that VIT1 was responsible for the provascular localization of Mn in the absence of MTP8.

Complementation of Fe Sensitivity in Yeast by Heterologous Expression of *MTP8*

Previously, it has been shown that the characteristic accumulation of Fe in provascular strands is completely

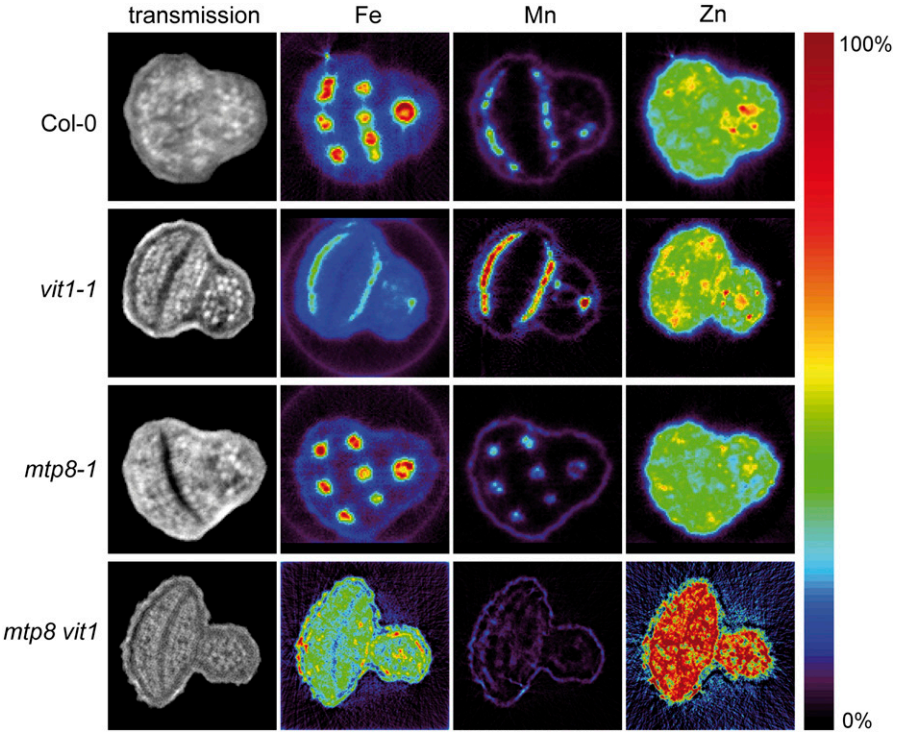

Figure 3. μXRF tomographs of intact seeds from wild-type, *mtp8-1*, *vit1-1*, and *mtp8 vit1* (*mtp8-1 vit1-1*) plants. Tomographs show absolute abundances of individual metals. Seeds were obtained from plants propagated under identical conditions. Three different seeds from each line were analyzed and representative images are shown. The color scale ranges for the individual metals are as follows: Fe, 0 to 1,200 $\mu g\ g^{-1}$; Mn, 0 to 1,100 $\mu g\ g^{-1}$; Zn, 0 to 500 $\mu g\ g^{-1}$.

disrupted in *vit1* embryos (Kim et al., 2006), as Fe is relocated to the sites of Mn accumulation via a mechanism that has remained largely elusive. Our observation that MTP8 is responsible for the defined localization of Mn (Fig. 3) that is shared by Fe in the absence of VIT1 (Kim et al., 2006) suggested that MTP8 may also transport Fe. To test vacuolar Fe transport competence, we expressed *MTP8* in the Fe-hypersensitive yeast strain *ccc1Δ*. In yeast, CCC1 (Ca^{2+}-sensitive Cross-Complementer 1) functions as a vacuolar Fe transporter required for survival on media containing elevated Fe concentrations (Li et al., 2001). As expected, growth of *ccc1Δ* on medium containing 5 mM Fe was strongly suppressed (Fig. 4). However, the expression of *MTP8* fully restored growth of *ccc1Δ* cells back to wild-type levels. This result indicated that besides Mn (Eroglu et al., 2016), MTP8 is also able to transport Fe.

Localization of Fe in Mature Embryos of *mtp8* and *vit1* Single and Double Knockout Lines

In addition to μXRF analyses, we visualized Fe distribution in embryos by Perls'/DAB staining to investigate the contribution of MTP8 to Fe allocation. In both *mtp8* mutant lines, Fe localized to the vascular strands, as it did in wild-type plants (Fig. 5A), indicating that MTP8 did not affect localization of the major stainable Fe reserves in the embryo. As reported previously (Roschzttardtz et al., 2009), absence of VIT1 resulted in a loss of Fe accumulation in the vascular strands. In addition, a closer look revealed that in *vit1* mutants, Fe staining was more pronounced in cortical cells of the hypocotyl and in particular on the upper, that is, abaxial side of the cotyledons (Fig. 5B). Hypothesizing that, in *vit1*, MTP8 may determine Fe localization on the abaxial side of the cotyledons, we reexamined *MTP8* promoter activity by focusing on abaxial and adaxial sides of the cotyledons. In agreement with the GUS reporter study (Fig. 1), *promoterMTP8*-dependent EYFP fluorescence confirmed the tissue-specific promoter activity of *MTP8* but further revealed that *MTP8* promoter activity is higher on the abaxial side of cotyledons (Fig. 5C). This localized expression pattern of *MTP8* coincided directly with the Fe distribution in *vit1* mutants, which appeared strongest and in well-defined spots on the abaxial side of cotyledons (Figs. 2, 3, and 5A).

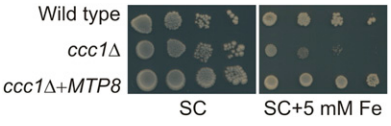

Figure 4. MTP8 complements a yeast mutant defective in vacuolar Fe transport. Overnight cultures of the wild-type strain BY4741 and the deletion mutant *ccc1Δ* harboring the empty vector pFL61 or pFL61-MTP8 were serially diluted and dropped onto plates containing either SC medium or SC medium supplemented with 5 mM $FeCl_2$.

We then took transversal and longitudinal sections of Perls'/DAB-stained seeds, which allowed defining Fe localization to the subepidermal layer on the abaxial side of *vit1-2* cotyledons and to both cortical cell layers of the hypocotyl (Fig. 6A). In contrast, the predominant localization of Fe to endodermal cells around the vascular strands remained unchanged in *mtp8-1* seeds. In the *mtp8 vit1* double mutant, well-defined Fe spots on the abaxial sides of the cotyledons and in the hypocotyl disappeared. Instead, Fe showed rather a dispersed distribution throughout all cell types of the different embryo tissues (Figs. 5A and 6A), confirming the μXRF analysis (Fig. 3). This was not a consequence of a smaller Fe reserve in *mtp8 vit1* seeds, in which Fe concentration and thousand seed weight were highly similar as in the other lines (Supplemental Fig. S2). To confirm the impact of MTP8 on subcellular Fe localization, we focused on subepidermal cells of *vit1-2* cotyledons (Fig. 6B). There, Perls'/DAB staining labeled Fe only in a central part of the cells, which most likely reflected Fe accumulation in the vacuole. This particular subcellular staining pattern was lost in the *mtp8 vit1* double mutant. Altogether, these observations indicated that in the absence of VIT1, MTP8 is responsible for the preferential localization of Fe on the abaxial side of the cotyledons, and that beyond VIT1 and MTP8 there is no further transport step responsible for cell type-specific accumulation of Fe in the embryo.

Involvement of MTP8 in Fe Reallocation during Seed Imbibition and Germination

The MTP8-dependent local accumulation of Mn in seeds suggested that MTP8 plays a role during seed development and/or during the early phase of seed germination. As active metabolism in a mature embryo is suspended during desiccation but restarts with imbibition (Bewley, 1997), we investigated whether *MTP8* expression is induced upon seed imbibition. When seeds were imbibed for 3 or 5 d but kept at 4°C to prevent germination, *MTP8* promoter activity strongly increased and showed a punctate pattern in cotyledons and the hypocotyl (Fig. 7A). This pattern was retained after 1 d of germination, whereas 1 d later *MTP8* promoter activity ceased. After 3 d of imbibition of wild-type seeds, Perls'/DAB-stained Fe mainly localized to the provascular strands of the cotyledons (Fig. 7B). In addition, Fe appeared in clearly defined spots on the abaxial but not on the adaxial side of the cotyledons, coinciding spatially with the expression pattern of the *MTP8* promoter (Fig. 5C). Transversal sections confirmed that these spots corresponded to the subepidermal layer on the abaxial side of the cotyledons (Fig. 7C). Counting the number of Fe hotspots over time confirmed a marked and steady increase of their appearance over the first 5 d of imbibition (Fig. 7D). In *mtp8-1* seedlings, no hotspots of Fe were observed. Monitoring Fe reallocation through imbibition up to 2 d of germination showed that in wild-type seedlings the

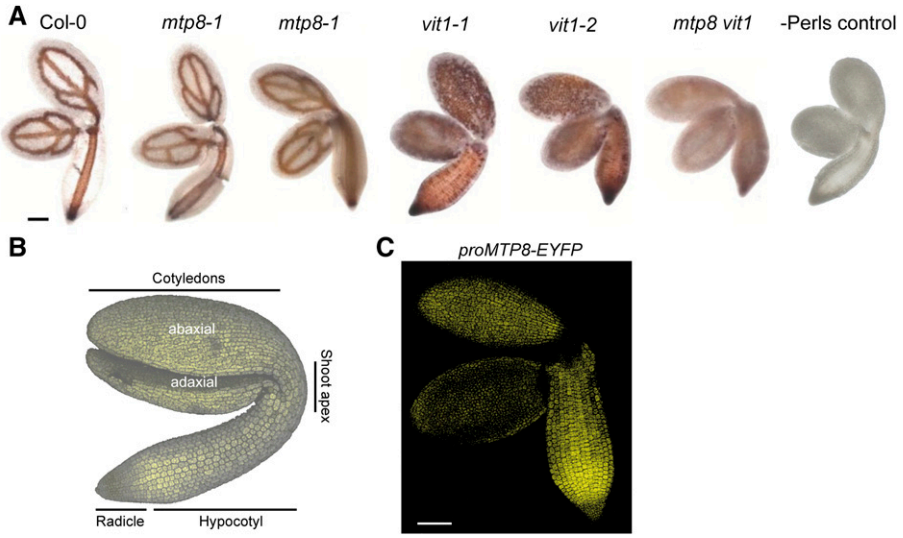

Figure 5. Impact of MTP8 and VIT1 on Fe distribution in embryos and expression of *EYFP* driven by the *MTP8* promoter. A, Perls'/DAB-stained Fe in postmature embryos isolated from seeds of wild-type, *mtp8-1*, *mtp8-2*, *vit1-1*, *vit1-2*, *or mtp8 vit1* (*mtp8-1 vit1-2*) double mutant plants. Mature seeds were incubated for 12 h in distilled water before embryos were isolated, stained by Perls'/DAB, and observed under a light microscope. B, Confocal image with autofluorescence of an Arabidopsis embryo. C, Embryos of *PromoterMTP8:EYFP* lines were imbibed in water for 24 h, isolated, and the EYFP-dependent fluorescence analyzed by a laser-scanning confocal microscope. Scale bars in A and C represent 100 μm.

vascular localization of Fe mostly disappeared (Fig. 7E). However, in *mtp8-1* seedlings Fe reallocation from the vascular tissue was retarded. Thus, during imbibition and early germination Fe is remobilized in an MTP8-dependent manner, and this remobilization coincided with Fe depletion from the vasculature.

Impact of MTP8 during Seed Imbibition and Germination in the Presence of Mn

In roots, MTP8 has been shown to confer tolerance to excess external Mn (Eroglu et al., 2016), raising the question whether such a tolerance mechanism is also relevant during imbibition or germination. Indeed, *mtp8-1* seeds were more sensitive to elevated Mn concentrations in the germination medium than the wild type, resulting in poor seedling development (Supplemental Fig. S3). To examine a role of MTP8 during imbibition, seeds were exposed to elevated concentrations of Mn for up to 72 h, washed to remove Mn from the seed coat, and germinated on 0.5× Murashige and Skoog (MS) medium, which contained 40 μM Mn (Fig. 8A). Regardless of the external Mn concentration during imbibition, wild-type seeds germinated properly and young seedlings did not show any visible phenotype. However, when imbibed in the presence of 500 μM Mn, *mtp8-1* seedlings developed chlorotic leaves, and exposure to an

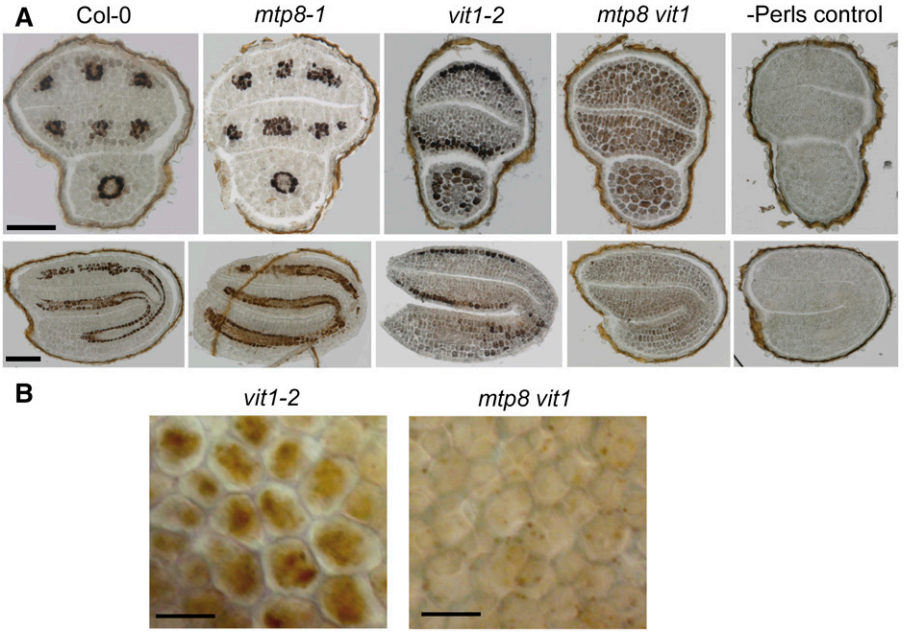

Figure 6. MTP8-dependent cell type-specific and subcellular Fe localization. A, Cell type-specific localization of Fe in cross sections through postmature embryos of wild-type, *mtp8-1*, *vit1-2*, or *mtp8 vit1* (*mtp8-1 vit1-2*) plants. Embryos were subjected to in situ Perls'/DAB staining. Perls control was stained only with DAB. B, Perls'/DAB-stained Fe in subepidermal cells of cotyledons of *vit1-2* or *mtp8 vit1* embryos. Scale bars represent 100 μm (A) or 20 μm (B).

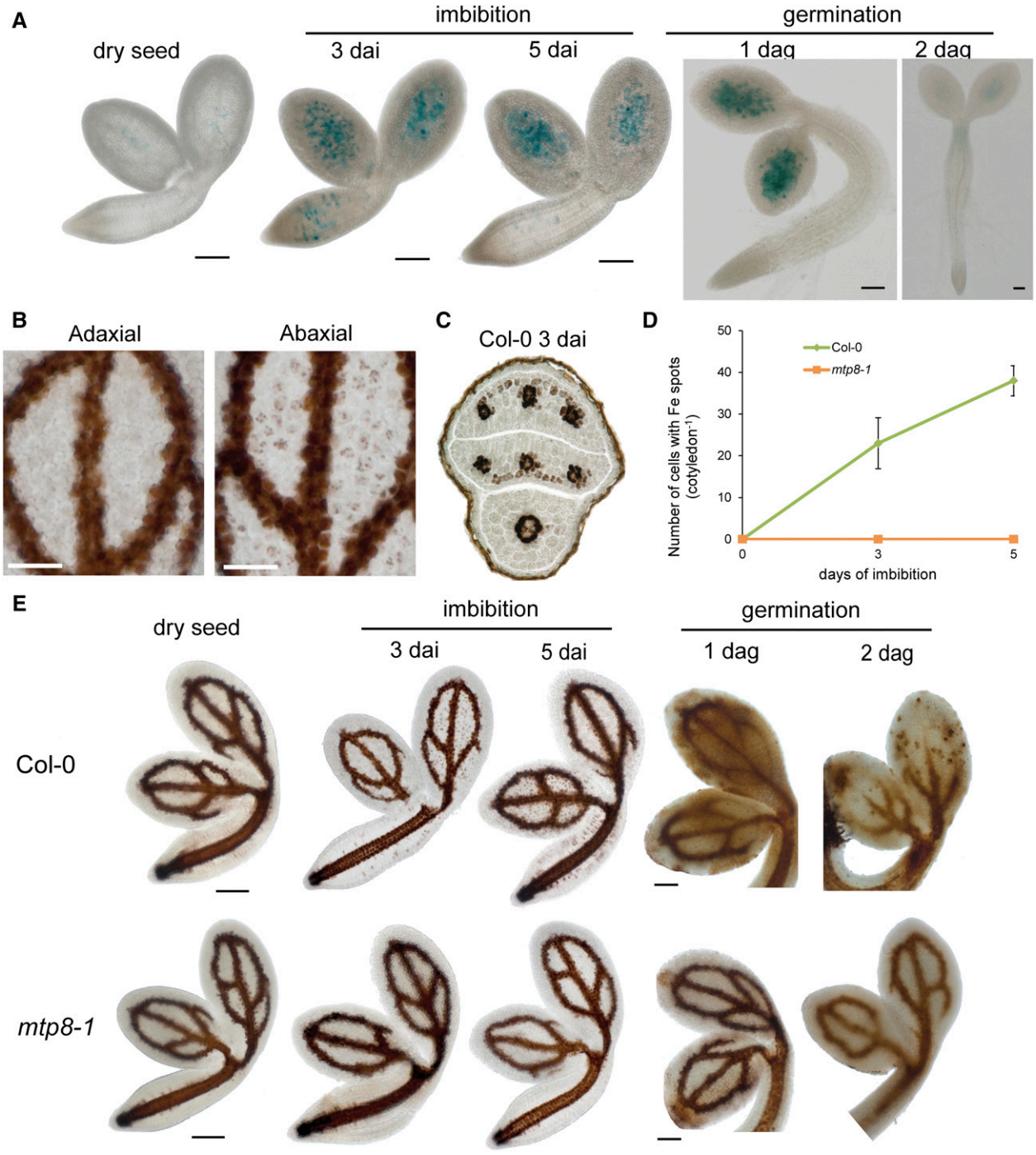

Figure 7. *MTP8* promoter activity and MTP8-dependent Fe accumulation on the abaxial side of cotyledons during seed imbibition and germination. A, Time-course analysis of *PromoterMTP8-GUS* activity during imbibition and germination. B, Perls'/DAB-stained Fe on the adaxial and abaxial side of the same cotyledon of wild-type embryos upon 3 d of imbibition. C, Perls'/DAB-stained Fe distribution in a cross section of a postmature wild-type embryo imbibed in water for 3 d. D, Quantification of Fe spots on the abaxial side of Col-0 and *mtp8-1* cotyledons after 0, 3, or 5 d of imbibition. Bars represent means ± SD; $n = 3$ embryos. E, Fe localization in cotyledons of wild-type and *mtp8-1* embryos during imbibition and germination. Isolated embryos or germinating seedlings were stained by Perls'/DAB and imaged under a microscope. Scale bars represent either 50 μm (C) or 100 μm (A, B, and E).

even higher Mn concentration strongly inhibited seedling growth and germination rate of seeds. To better understand the role of MTP8 in Mn absorption by imbibed seeds, Mn-exposed wild-type and *mtp8-1* mutant seeds were subjected to elemental analysis. In the absence of Mn, Mn levels in *mtp8-1* seeds were lower

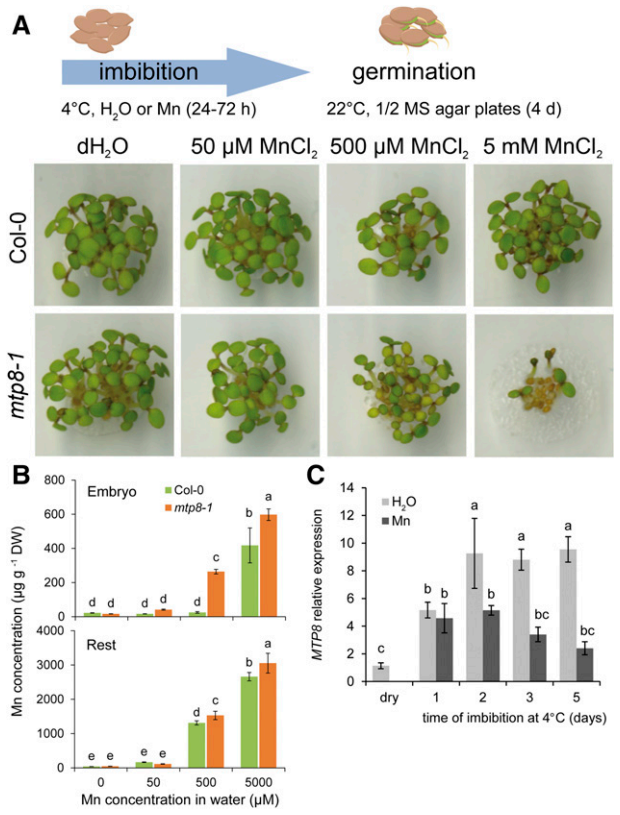

Figure 8. Effect of Mn availability during seed imbibition on germination and *MTP8* expression in wild-type and *mtp8-1* seeds. A, Seeds were imbibed in distilled water (dH_2O) or in 50, 500 μM, or 5 mM $MnCl_2$ at 4°C for 3 d. Then, imbibed seeds were washed with water and germinated on 0.5× MS agar containing 40 μM $MnCl_2$ for 4 d before photos were taken. B, Mn concentrations in wild-type or *mtp8-1* embryos or the seed coat with remaining seed constituents (rest) after isolation of embryos. C, Time-course analysis of *MTP8* transcript levels during imbibition at 4°C in distilled water or in water containing 5 mM $MnCl_2$ (Mn). Bars represent means ± SD; $n = 3$ biological replicates. Different letters indicate significant difference according to Tukey's test ($P < 0.05$).

(Supplemental Fig. S4). Over a period of 72 h in the presence of Mn, Mn concentrations in the seeds of both lines increased. Unexpectedly, at 0.5 and 5 mM external Mn, Mn accumulation was even higher in *mtp8-1* than in wild-type seeds. We then separated embryos from the rest of the seed and observed that *mtp8-1* embryos accumulated more Mn than wild-type embryos, suggesting that Mn concentrations in the embryo tissue reached toxic levels earlier in the absence of MTP8 (Fig. 8B). Accumulation of Mn in the embryo coincided with an increase of *MTP8* transcript levels already after 1 d of imbibition when seeds were imbibed in water (Fig. 8C). In the presence of 5 mM Mn, *MTP8* transcript levels remained lower and ceased earlier. With regard to the induction of *MTP8* upon imbibition and similar Mn concentrations in embryos of both lines at 5 mM external Mn (Fig. 8B), poor germination of *mtp8-1* seeds suggested that a larger cytosolic Mn fraction in *mtp8-1* embryos conferred higher sensitivity to external Mn.

Ecophysiological Role of MTP8 in Metal Homeostasis during Wet-Dry Cycles

In temperate and cold climates, seed imbibition without an onset of germination plays an important role during autumn or winter, especially when seeds remain buried in cold soils and are exposed to repeated wet-dry cycles due to fluctuating water conditions. To address a role of MTP8 in metal homeostasis under such conditions that augment plant-available Mn pools, we exposed seeds at 4°C to wet-dry cycles in a peat-based substrate supplemented with different amounts of Mn. One set of substrate was kept dry and another set water saturated. In 3-d intervals, seeds contained inside nylon mesh bags were transferred from wet to dry substrate and vice versa (Fig. 9A), and 21 d after starting the experiment seeds were finally transferred for germination onto control substrate without Mn supplementation.

When kept in control substrate (0.1 g kg^{-1} Mn), germination rates of *mtp8* seeds were indistinguishable from those of wild-type seeds, while after exposure to substrate containing 10 g kg^{-1} Mn during imbibition *mtp8* seeds germinated with a delay (Fig. 9, B and C). At the highest Mn availability in the substrate (50 g kg^{-1} Mn), germination of all seeds was delayed or completely inhibited. Nonetheless, 70 to 80% of Col-0 and *vit1* seeds had germinated after transfer to control conditions (Fig. 9D). At the same time point, germination of *mtp8 vit1* and of the two single mutant seeds still remained very poor. Notably, even when able to germinate after 8 d, the seedlings of both *mtp8* and *mtp8 vit1* mutants produced less biomass than those of Col-0 and *vit1-2* (Fig. 9E). These results pointed to a critical role of MTP8 but not of VIT1 in Mn homeostasis during the pregermination phase under fluctuating water conditions in solid growth substrates.

Contribution of MTP8 to Mn Storage in Seeds

To test the hypothesis whether MTP8 also affects Mn storage in seeds and subsequent seed germination in the long run, we grew Col-0 and *mtp8* plants on Mn-free or Mn-supplemented perlite to maturity before recording the germination rate of their seeds. Under conditions of sufficient Mn supply, seed yield and Mn concentrations were similar in all genotypes (Fig. 10, A and B). In contrast, Mn limitation in the substrate markedly reduced seed yield and seed Mn concentrations, but not Fe concentrations (Fig. 10C). The decrease of seed Mn concentrations in Mn-deficient plants was more pronounced in *mtp8* seeds (Fig. 10B). As expressed in delayed germination and lower germination rates, seeds harvested from plants grown without Mn supplementation germinated poorly (Fig. 10, D and E). This effect was even more prominent in *mtp8* seeds, showing that MTP8-dependent seed reserves of Mn are essential for adequate germination.

DISCUSSION

Transport processes of metal micronutrients to and within seeds are a prerequisite for seed development

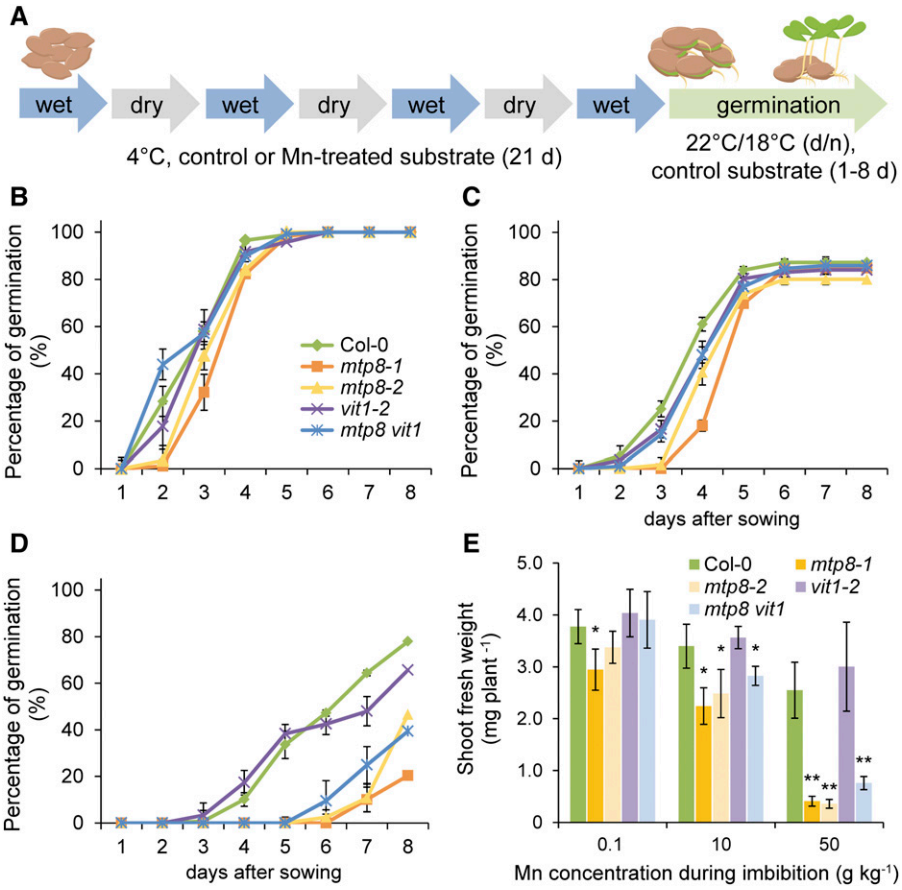

Figure 9. MTP8-dependent germination after exposure of seeds to Mn during wet/dry cycles. A, Schematic representation of wet/dry cycles under low temperature. Dormant seeds of wild type (Col-0), *mtp8-1*, *mtp8-2*, and *mtp8 vit1* (*mtp8-1 vit1-2*) were planted in a peat-based substrate supplemented or not with $MnCl_2$ and maintained at 4°C for 21 d. Seeds were exposed to alternating wet and dry cycles as indicated and then allowed to germinate in control substrate. B to D, Germination rate after wet-dry cycles at 4°C in substrate containing 0.1 (B), 10 (C), or 50 (D) g kg^{-1} $MnCl_2$. Symbols represent means ± SD; $n = 4$ replicates with >15 seeds. E, Shoot fresh weight of seedlings exposed to different Mn concentrations during wet/dry cycles at 4°C before germinating in substrate containing 0.1 g kg^{-1} $MnCl_2$. Fresh weight was determined 12 d after sowing. Bars represent means ± SD; $n = 4$ replicates each consisting of 5 to 7 plants. * or ** indicates significant differences from Col-0 according to pairwise *t* test at $P < 0.05$ or $P < 0.001$, respectively.

and subsequent germination, as well as for micronutrient enrichment in seed-based food. Moreover, in oleiferous seeds of soybean (*Glycine max*), oilseed rape (*Brassica napus*), or Arabidopsis, metal micronutrients take over additional, specific roles, such as in oil biosynthesis, which strongly depends on Mn (Wilson et al., 1982). Apart from processes regulating metal delivery to seeds, storage capacities and reallocation processes within seeds are decisive for germination success and subsequent seedling vigor (Eggert and von Wirén, 2013, 2015). At the subcellular level, the vacuole in particular creates an important sink for Fe and Mn during seed development and provides an essential source for these metals during the early germination phase. Regarding Fe, these functions are mediated by the vacuolar Fe importer VIT1 (Kim et al., 2006; Roschzttardtz et al., 2009) and the vacuolar exporter pair NRAMP3/NRAMP4 (Lanquar et al., 2005), which together constitute a functional module for Fe storage in and release from endodermal cells of the Arabidopsis embryo (Mary et al., 2015). In the case of Mn, the transporters responsible for vacuolar Mn loading and unloading during seed development and germination have remained unknown. Here, we report that the vacuolar Mn transporter MTP8 is responsible for a characteristic enrichment of Mn in cortical cells of the hypocotyl and in subepidermal cells of cotyledons as well as for Mn homeostasis during imbibition and germination under fluctuating water conditions. Moreover, MTP8 is also involved in vacuolar Fe loading not only as a default option in the absence of VIT1, but also for Fe reallocation during the pregermination phase. This study identifies MTP8 as one essential component of the predicted "Mn/Fe importer-exporter module" located in vacuoles of subepidermal cells of cotyledons and cortical cells of the hypocotyl, which regulates homeostasis of Mn and reallocation of Fe in embryos and germinating seedlings.

Mn Accumulation in the Embryo Depends on MTP8

An elemental analysis of Arabidopsis seeds during their development showed that Mn accumulated up to the early bent stage almost exclusively in the endosperm and seed coat but only very little in the embryo, while with progression to late bent stage and maturity translocation of Mn from the endosperm into the embryo set in (Otegui et al., 2002). This temporal pattern coincided with the disappearance of Mn crystals from the endosperm (Otegui et al., 2002) and with the onset of *MTP8* promoter activity in the embryo (Fig. 1). In the embryo, *MTP8* promoter activity was predominant on the abaxial side of the cotyledons (Fig. 5C), which corresponded precisely to the site of Mn accumulation in

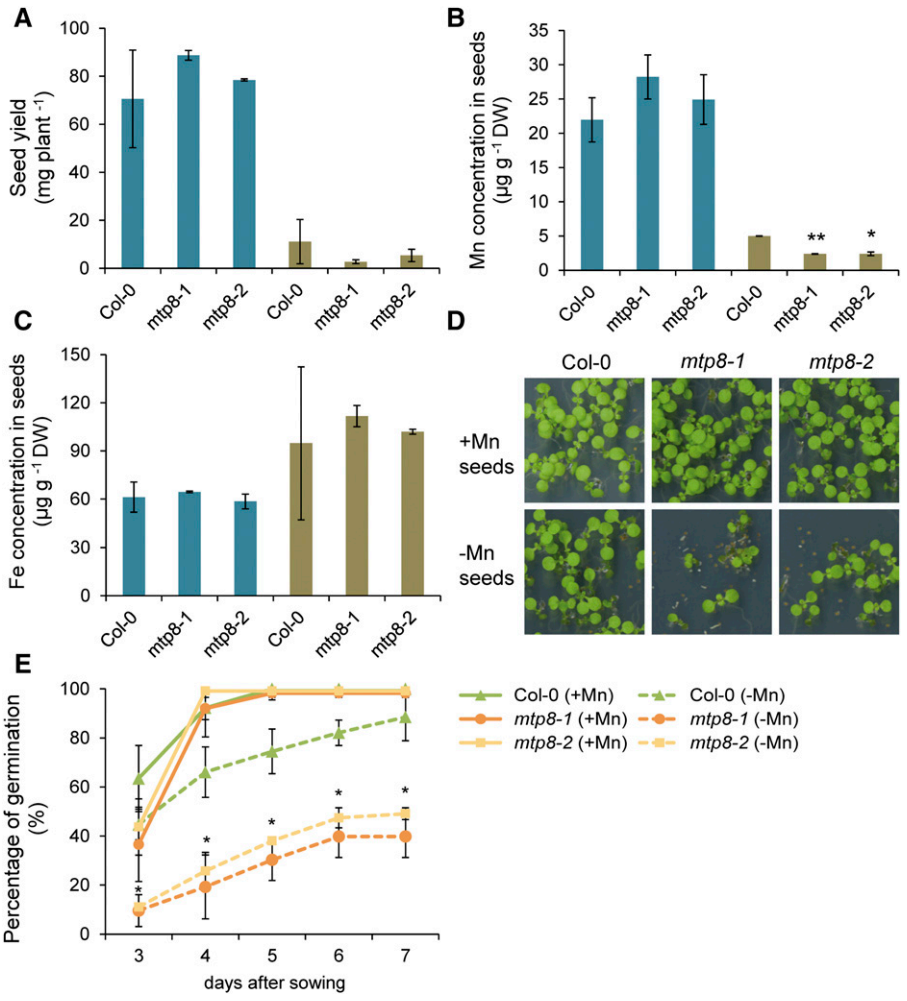

Figure 10. Influence of MTP8 on seed yield, seed Mn concentration, and seed vigor under Mn-limiting growth conditions. A to C, Mother plants were grown on perlite supplemented with 5 μM $MnCl_2$ (+Mn) or without Mn supply (−Mn). A, Seed yield and seed concentrations of Mn (B) and Fe (C) were assessed at maturity. Bars represent means ± SD; $n = 3$ biological replicates. Asterisks indicate significant differences to Col-0 according to Student's t test at $^*P < 0.01$ or $^{**}P < 0.001$, respectively. D and E, Germination of seeds harvested from plants grown on perlite supplemented with 5 μM Mn (+Mn) or without Mn supplementation (−Mn). D, Germination assay and (E) proportion of germinated seeds as scored 3 to 7 d after sowing on 0.5× MS containing 40 μM Mn. Symbols represent means ± SD; $n = 3$ biological replicates. Asterisk indicates significant differences between Col-0 and *mtp8-1* as well as *mtp8-2* in the +Mn or –Mn treatment.

dry seeds (Figs. 2 and 3). As verified directly by μXRF (Figs. 2 and 3) and indirectly by MTP8-dependent Fe localization (Figs. 5 and 6), the site of *MTP8* expression and Mn localization was consistent with the subepidermal cell layer of the abaxial side of cotyledons and with cortical cells of the hypocotyl. In the hypocotyl, MTP8 conferred metal accumulation in irregularly distributed hot spots. Since this cell type-specific pattern of Mn accumulation was completely absent in seeds of the two *mtp8* single mutants or the *mtp8 vit1*

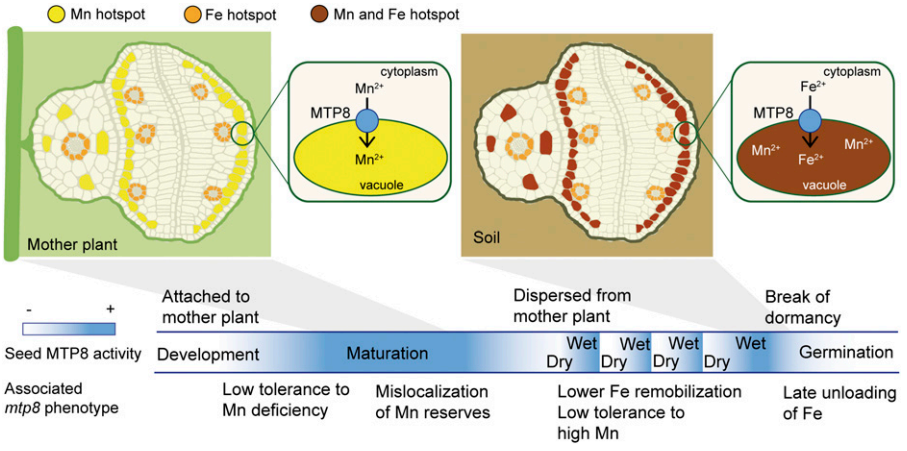

Figure 11. Schematic model for the role of MTP8 in vacuolar metal transport in embryos during seed development and during imbibition of seeds in the soil.

double mutant (Figs. 2 and 3), the major driving force for subepidermal and cortical Mn accumulation in the embryo depends on MTP8 (Fig. 11). With respect to its ability to compartmentalize Mn to the vacuole (Eroglu et al., 2016), MTP8 is able to create a strong sink for Mn in subepidermal cells. Following the common route for assimilates and minerals, Mn unloaded from the phloem of the mother plant may move via the outer integument toward the endosperm and the embryo (Stadler et al., 2005). After crossing the plasma membrane of embryonic cells, an MTP8-mediated accumulation of Mn in the subepidermal layer of the cotyledons may allow efficient withdrawal of Mn from the seed coat, which is left with ~10% of the overall seed Mn in oilseed rape (Eggert and von Wirén, 2013). However, the physiological function of this cell type-specific Mn localization in the abaxial side of cotyledons is not yet clear. One possibility is that subepidermal Mn is associated with photosynthetic activity in cotyledons, since Mn is a key element in the water-splitting system of PSII. In soybean embryos, a strong gradient in PSII activity forms between the abaxial and the adaxial sides of cotyledons as development progresses (Borisjuk et al., 2005). During the late storage phase, considerable PSII activity was still detected on the abaxial side of the cotyledons, whereas PSII activity ceased completely on the adaxial side. Assuming a similar pattern of PSII activity also in Arabidopsis embryos, the comparatively late activation of the *MTP8* promoter during embryo development (Fig. 1) may indicate that MTP8 is involved in sequestering Mn released from chloroplasts during late PSII disintegration on the abaxial side of cotyledons.

MTP8 Assures Mn Homeostasis during Seed Development and Germination

The physiological context in which MTP8 functions in seeds is completely different from its role in vegetative organs. In Stylosanthes, rice (*Oryza sativa*), barley, and Arabidopsis, evidence has been provided that MTP8 proteins confer tolerance to Mn toxicity (Chen et al., 2013; Delhaize et al., 2003; Pedas et al., 2014, Eroglu et al., 2016). In Arabidopsis roots, this function has been set into context with Fe deficiency. Fe deficiency-induced expression of the poorly substrate-specific Fe^{2+} transporter IRT1 provokes cellular overload with Mn, which suppresses activity of the membrane-bound ferric Fe chelate reductase (Eroglu et al., 2016). Concomitant induction of MTP8 then allows compartmentalization of excess Mn into the vacuole sustaining not only reductase activity but also a balanced translocation of Fe and Mn to the shoot. Thus, in roots MTP8 belongs to a group of vacuolar metal loaders, also including MTP3 and IREG2 (Arrivault et al., 2006; Schaaf et al., 2006), which are under transcriptional control of the Fe deficiency-induced regulator FIT (Colangelo and Guerinot, 2004) and localized to outer root cells where Fe acquisition takes place.

Based on its vacuolar transport function for Mn, MTP8 can also contribute to Mn storage in seeds. Expression of *MTP8* is confined to later developmental stages, when the embryo has already expanded its cotyledons (Fig. 1). This limited time span severely restricts the period of MTP8-mediated Mn loading to the abaxial side of the cotyledons, eventually partitioning in this region one-third of the total Mn reserves of the embryo (Schnell Ramos et al., 2013). Nevertheless, wild-type and *mtp8* seeds showed highly similar and typical Mn concentrations of 20 to 30 $\mu g\ g^{-1}$ when grown with ample Mn supply (Fig. 10B). Based on the high affinity of Mn to form complexes with phosphate, heterometallic phytate complexes have been identified in acidic compartments of wheat (*Triticum aestivum*) seeds where Mn most likely enters a $MnZn_4$-inositol-6-phosphate complex (Rodrigues-Filho et al., 2005). However, intracellular localization and predominant binding forms may change under Mn-deficient growth conditions. When the growth substrate was not supplemented with Mn, seed yield of *mtp8* plants tended to drop, and Mn concentrations decreased to ~50% of those of the wild type (Fig. 10, A and B). In consequence, *mtp8* seeds showed a delay in germination and lower germination rates (Fig. 10, D and E). Previous studies pointed out that seeds with low Mn levels exhibit poor germination rates (Crosbie et al., 1993), which may be related to nonscavenged reactive oxygen species due to insufficient Mn for Mn-SOD synthesis (Martin et al., 2013). Thus, our results indicate that MTP8 takes over a function in safeguarding seed viability by increasing the stored Mn pool in the embryo, which is of particular relevance when the mother plant suffers from Mn deficiency.

Vacuolar sequestration of Mn by MTP8 is also important for seed performance if external Mn availability is high. While water logging may increase Mn levels in the soil solution to >0.5 mM (Gilmour, 1977), simultaneous presence of organic matter may enhance Mn reduction and raise Mn concentrations even up to 2 mM (Porter et al., 2004). Germination in the presence of 1 mM external Mn or imbibition in 0.5 to 5 mM Mn prior to germination caused poor development and chlorotic appearance only of *mtp8* seedlings (Supplemental Fig. S3; Fig. 8A), which coincided with higher accumulation of Mn in *mtp8* embryos (Fig. 8B). Thus, expression of MTP8 shortly after imbibition (Fig. 8C) most likely protects the developing seedling from excess cytosolic Mn due to vacuolar sequestration. Higher Mn accumulation in *mtp8* seeds and embryos at elevated external Mn was unexpected, as MTP8 was supposed to create a vacuolar sink favorable for Mn accumulation. Under these conditions, MTP8-dependent vacuolar compartmentalization may be involved in retrograde signaling between the vacuolar Mn store and Mn uptake across the plasma membrane in the embryo tissue.

Our experiments further added an ecophysiological dimension to the vacuolar loading function of MTP8, which may gain importance in autumn or winter when soil humidity allows seeds to imbibe water and restart

metabolic functions but the soil temperature is too low to allow germination. Those wet and poorly aerated soil conditions cause a decline of the redox potential of the soil solution, thereby mobilizing sparingly soluble Mn oxides and increasing Mn availability. Such conditions were simulated by subjecting seeds to repeated wet-dry cycles at 4°C (Fig. 9A). When Mn concentrations in the substrate were high, the loss of MTP8 resulted in severe defects in seed germination and seedling establishment (Fig. 9, B–E), indicating that seeds must actively maintain metal homeostasis also after detachment from the mother plant. Whereas during seed development the amount of nutrients that eventually reaches the seed is controlled by multiple transport steps in the mother plant (Stacey et al., 2008; Curie et al., 2009; Olsen et al., 2016), dispersed seeds are directly exposed to elements contained in the soil. Although the seed coat offers a protective barrier to otherwise uncontrolled nutrient intake, the efficacy of such protection depends on the plant species and the element in question (Seregin and Kozhevnikova, 2005; Wierzbicka and Obidzińska, 1998). Our results suggest that MTP8 represents a mechanism to prevent deleterious effects that may arise from exposition of dispersed seeds to elevated soil metal concentrations. MTP8-mediated transport functions are thus expected to gain relevance in temperate and cold climates, when imbibed seeds can remain buried in wet or temporally waterlogged soils.

MTP8 Is Part of a Module of Tonoplast Transporters Regulating Fe and Mn Homeostasis in Seeds

Although primarily involved in Mn localization in developing embryos, MTP8 becomes a major vacuolar Fe transporter in the absence of VIT1. This conclusion is supported by (1) the ability of MTP8 to mediate Fe detoxification in yeast (Fig. 4); (2) MTP8-dependent intracellular, presumably vacuolar localization of Fe in the absence of VIT1 (Fig. 6B); (3) the overlap between the domain of *MTP8* promoter activity on the abaxial side of cotyledons and the major site of Fe accumulation in postmature *vit1* embryos (Figs. 2, 3, and 5, A and C); and (4) the loss of subepidermal Fe localization in *mtp8 vit1* embryos (Figs. 3 and 6). Previously, it has been shown by a yeast complementation assay and the positive correlation between *MTP8* expression and tissue Mn accumulation in planta that MTP8 can transport Mn (Eroglu et al., 2016). Here, we show that the metal transport function of MTP8 extends to Fe. This finding is intriguing, since Mn-CDFs have been described to be specific for Mn (Migeon et al., 2010; Montanini et al., 2007; Peiter et al., 2007).

In embryos, the activity of VIT1 during seed development concentrates Fe predominantly in endodermal cells that surround the vasculature (Kim et al., 2006; Roschzttardtz et al., 2009). If VIT1 is lost, Fe accumulates in cortical cells of the hypocotyl and in subepidermal cells of cotyledons (Fig. 4A; Roschzttardtz et al., 2009; Mary et al., 2015). These alternative sites of Fe accumulation coincide with the domains of *MTP8* expression in embryos (Fig. 5C). Interestingly, when both *VIT1* and *MTP8* are disrupted, Fe diffusely accumulates in all cells (Figs. 3, 5A, and 6A). Thus, MTP8 is the transporter responsible for cell type-specific reallocation of Fe in *vit1* embryos. Noteworthy, this study also raised evidence that MTP8 functions in reallocating Fe in the presence of VIT1. According to Perls'/DAB staining of imbibed seeds, Fe starts concentrating on the abaxial side of cotyledons in an MTP8-dependent manner as seeds take up water (Fig. 7, B and C). This coincides with enhanced *MTP8* promoter activity during imbibition (Fig. 7A). Thus, cell type-specific expression of MTP8 defines a transient vacuolar storage site for Fe mobilized during imbibition and prior to germination (Fig. 11), which may protect cells from the formation of reactive oxygen species.

In wild-type seeds, the release of Fe from vacuoles during germination is mediated by NRAMP3 and NRAMP4, and the absence of both transporters results in poor seedling development under low Fe availability (Lanquar et al., 2005). In line with this function, Fe is retained in endodermal cells of *nramp3nramp4* double mutants during seed germination and seedling establishment, indicating that VIT1, NRAMP3, and NRAMP4 form a functional module active in endodermal cells surrounding the vasculature (Mary et al., 2015). Intriguingly, NRAMP3 and NRAMP4 activity is not essential for Fe mobilization if Fe is not concentrated in endodermal cells, as *nramp3 nramp4 vit1* triple mutants are able to efficiently mobilize Fe and show no visible phenotypes when germinated on low Fe conditions (Mary et al., 2015). This indicates that MTP8-supplied Fe stores in *vit1* embryos are not remobilized by NRAMP3 and NRAMP4. As subepidermal cells of cotyledons and cortical cells of hypocotyl provide the alternative route for Fe storage, these cells must harbor another vacuolar Fe importer-exporter module. As shown here, this module comprises of MTP8 and a yet unknown vacuolar unloader for Fe (Fig. 11).

Apart from the fact that MTP8 mediates Fe transport in *vit1* embryos, our results also reveal another level of interplay between VIT1 and MTP8, as μXRF analyses showed that in *mtp8* embryos Mn is concentrated predominantly around the vasculature (Figs. 2 and 3), where VIT1 is expressed (Kim et al., 2006). In fact, the pattern of Mn distribution in *mtp8* embryos closely matches that of Fe accumulation, suggesting that VIT1 may indeed act as a default pathway for Mn accumulation in embryos in the absence of MTP8. In this regard, it has been shown previously that, besides Fe, VIT1 can also transport Mn when expressed in yeast cells (Kim et al., 2006).

Taken together, we demonstrate that MTP8 plays a critical role in Mn accumulation in seeds by creating a vacuolar sink in the embryo, which is of particular importance when plants are grown under low Mn availability. In embryos, MTP8 defines the major sites of Mn accumulation in cortical cells of the hypocotyl and in the subepidermal cells of the abaxial side of

cotyledons. Once detached from mother plants, seeds take up Mn from the environment during seed imbibition, and MTP8 sequesters Mn after excessive intake to prevent the embryo from cytotoxicity. Moreover, the transport function of MTP8 extends to Fe as it reallocates Fe in embryos in the absence of VIT1 during embryo development. During imbibition MTP8 acts in the presence of VIT1 and creates a transient Fe sink in subepidermal cells of the cotyledons, which promotes the subsequent release of Fe from the vasculature. With these seed-specific Fe transport properties MTP8 may also represent an attractive target in biofortification strategies aiming at the enhancement of micronutrient contents in seeds (White and Broadley, 2009; Bouis et al., 2011; Ricachenevsky et al., 2013; Vatansever et al., 2017).

MATERIALS AND METHODS

Plant Materials and Plant Growth Conditions

All Arabidopsis (*Arabidopsis thaliana*) lines used in this study were derived from Columbia-0. *vit1-1* (SALK_020596C) and two *promoterVIT1:GUS* lines (Kim et al., 2006) were obtained from Mary-Lou Guerinot (Dartmouth College). The transgenic lines *mtp8-1*, *mtp8-2*, *35S:MTP8#OE2*, *promoterMTP8:GUS*, and *promoterMTP8:EYFP* have been described previously (Eroglu et al., 2016). The *vit1-2* (SALK_123591C) T-DNA insertion line was identified from the SALK collection. To obtain *mtp8 vit1* double mutants, *mtp8-1* was crossed with either *vit1-1* or *vit1-2*, and selection of homozygous plants at the two loci was carried out by PCR in the F2 progeny.

For long-term growth experiments under variable Mn availability, we followed the growth conditions described in (Lanquar et al., 2010). Briefly, perlite was washed with 2 mM EGTA and 15 volumes of deionized water. Seeds were directly sown on perlite. Plants were cultivated under long-day conditions (16 h light/8 h dark) and were regularly watered with a modified Hoagland's solution containing 0.28 mM KH_2PO_4, 1.25 mM KNO_3, 0.75 mM $MgSO_4$, 1.5 mM $Ca(NO_3)_2$, 25 μM H_3BO_3, 50 μM KCl, 1 μM $ZnSO_4$, 0.1 μM Na_2MoO_4, 0.5 μM $CuSO_4$, 10 μM Fe-EDTA, and 3 mM MES-KOH (pH 5.6), and if not indicated otherwise 5 μM $MnSO_4$.

Seed Imbibition Experiments

An aliquot of seeds was submerged in 1.5-mL plastic tubes in distilled water with different concentrations of $MnCl_2$, as indicated in Figure 6 and Supplemental Figure S3. Tubes were incubated in the dark at 4°C for the indicated time. For germination tests, imbibed seeds were transferred to 0.5× MS medium without Suc and solidified with 1% (w/v) Difco agar (Becton Dickinson) immediately after being washed two times with distilled water. For the determination of metals, seeds were first desorbed to remove external contaminations (Cailliatte et al., 2010). Briefly, seeds were washed in 2 mM $CaSO_4$, 10 mM EDTA solution for 10 min and then in 0.3 mM bathophenanthroline disulphonate and 5.7 mM sodium dithionite for 3 min before being rinsed twice in deionized water. Embryos were recovered from the seeds by pressing seeds between two glass slides. Samples were dried at 65°C before elemental analysis.

μXRF

μXRF tomography of intact seeds was performed at beamline i18 of the Diamond Light Source Synchrotron (Didcot, UK) UK. Intact dry seeds were stuck into the open end of 0.3-mm polyimide capillaries. Measurements were performed with a 11.0-keV beam focused by a Kirkpatrick-Baez mirror system to ~2 μm, combined with fluorescence detection by a 6-element silicon drift detector plus a 4-element germanium detector coupled to Xpress-3 readout electronics. Flux behind the sample was measured with a PIPS diode for tomograms with absorption contrast. Samples were mounted on a rotating stage. Tomographic scans consisted of 360° of rotation in 2° steps, in each rotation step performing a line scan in 1-μm intervals. Integration time per point was 50 ms. To minimize thermal beam damage seeds were cooled with a cryostream to about 100K throughout the measurement. Frozen-hydrated multielement standards (containing 5 mM of each metal) filled into identical capillaries as used for mounting the seeds were measured in the same way as the seeds. The sinograms resulting from the measurements were reconstructed to tomograms using the CGLS algorithm. The resulting relative pixel intensities in the tomograms of Fe, Mn, and Zn were converted to $\mu g\ g^{-1}$ values according to the standards, after which 32-bit grayscale images were translated into a custom-defined color scale and converted to 24-bit RGB color images.

μXRF imaging of seed sections was carried out at the Super Photon Ring-8 facility in Hyogo, Japan. Details of the μ-XRF system have been reported by Kamijo et al. (2003) and Hokura et al. (2006). Elemental maps were obtained by scanning the samples with a 10.0-keV monochromatized beam. The monochromatized beam was focused by a Kirkpatrick-Baez mirror system into a 0.6-μm vertical direction × 0.7-μm horizontal direction microbeam at the sample position. Samples were exposed to the microbeam, and fluorescent x-rays emitted from the samples were detected using a silicon drift solid-state detector. To obtain two-dimensional images of Zn, Fe, and Mn in the samples, the sample stage was scanned along the x-y axes during fluorescent x-ray detection. The scanning step size was set to 2 μm. The x-ray fluorescence intensities were measured for 0.1 s per point. The integrated x-ray fluorescence intensity of each line was calculated from the spectrum and normalized to that of the incident beam, which was measured by an ionization chamber, and then the elemental maps of the measured areas were calculated. The x-ray fluorescence intensity in the μ-XRF analysis was directly proportional to the concentration of the element (Terada et al., 2010).

Elemental Analysis

Dried seed, seed parts, or whole shoots were weighed into PTFE digestion tubes and digested in HNO_3 under pressure using a microwave digester (UltraCLAVE IV; MLS). Elemental analysis of whole shoots was undertaken using inductively coupled plasma optical emission spectroscopy (iCAP 6500 dual OES spectrometer; Thermo Fisher Scientific), whereas seed fractions were analyzed by sector field high-resolution ICP-MS (ELEMENT 2; Thermo Fisher Scientific). In both cases, element standards were prepared from certified reference materials from CPI international.

Quantitative RT-PCR

RNA was isolated from seeds using Spectrum Plant Total RNA kit (Sigma-Aldrich) according to the manufacturer's instructions. Total RNAs were treated with RQ1 RNase-free DNase (Promega) and then reverse-transcribed into cDNA with the RevertAid First Strand cDNA Synthesis Kit (Fermentas), using oligo(dT) primers and following the manufacturer's instructions. Quantitative RT-PCR was performed using the CFX384 Touch Real-Time PCR Detection System (Bio-Rad) and iQ SYBR Green Supermix (Bio-Rad). Relative expression was calculated according to Pfaffl (2001) and normalized to the transcript levels of *PP2A* (At1g69960). A list of primers used in this study is shown in Supplemental Table S1.

Histochemical Analyses and Microscopy

Isolated embryos of *promoterMTP8:GUS* lines were incubated at 37°C in a GUS reaction buffer containing 0.4 g L^{-1} 5-bromo-4-chloro-3-indolyl-β-D-glucuronide, 50 mM sodium phosphate (pH 7.2), and 0.5 mM ferrocyanide. Whereas embryos in heart, torpedo, and walking stick stages were incubated overnight, incubation was limited to 2 h for embryos in green-cotyledon and postmature stages. Stained embryos were fixed in 2% formaldehyde and 2% glutaraldehyde in 50 mM cacodylate buffer (pH 7.2), dehydrated in an ethanol series (30%, 40%, … 100%), and embedded in Spurr's resin. Samples were imaged with a light microscope (Axioskop; Carl Zeiss).

Confocal images of *promoterMTP8:EYFP* embryos were acquired with a Zeiss LSM 780 microscope equipped with a 10×/0.45 M27 objective. EYFP-dependent fluorescence was detected by excitation at 488 nm with an argon laser and filtering the emitted light at 511 to 531 nm. The software ZEN (Zeiss) was used for adjustments and image recording.

Yeast Complementation

The yeast (*Saccharomyces cerevisiae*) deletion mutant Y04169 (*ccc1Δ*) and its reference strain BY4741 were obtained from the Euroscarf collection (Winzeler

et al., 1999). To construct the pFL61-MTP8 plasmid, the *MTP8* cDNA was amplified from Col-0 cDNA using *Not*I-containing primers and cloned into the yeast expression vector pFL61 (Minet et al., 1992) downstream of the *PGK* promoter. Yeast transformation was carried out according to Elble (1992). Transformants were selected on synthetic complete plates lacking the appropriate selective markers. Yeast drop assays were performed as described previously (Peiter et al., 2005).

Perls' Staining and DAB/H_2O_2 Intensification

Perls' staining and DAB/H_2O_2 intensification were performed according to Roschzttardtz et al. (2009). Embryos were dissected from seeds previously imbibed in distilled water for 3 h, using a binocular magnifying lens. The isolated embryos were vacuum-infiltrated with equal volumes of 4% (v/v) HCl and 4% (w/v) K-ferrocyanide (Perls' staining solution) for 15 min and incubated for 30 min at room temperature (Stacey et al., 2008). DAB intensification was applied as described by Meguro et al. (2007). After washing with distilled water, the embryos were incubated in a methanol solution containing 0.01 M NaN_3 and 0.3% (v/v) H_2O_2 for 1 h and then washed with 0.1 M phosphate buffer (pH 7.4). For the intensification reaction, the embryos were incubated between 10 and 30 min in a 0.1 M phosphate buffer (pH 7.4) solution containing 0.025% (w/v) DAB (Sigma-Aldrich), 0.005% (v/v) H_2O_2, and 0.005% (w/v) $CoCl_2$ (intensification solution). The reaction was stopped by rinsing with distilled water. For in situ Perls' staining, seeds were dehydrated in an ethanol series (30%, 40%, …, 100%) and embedded in wax. Then, 10-μm sections were cut and stained according to Roschzttardtz et al. (2009).

Accession Numbers

Sequence data from this article can be found in the GenBank/EMBL data libraries under accession numbers ■■■.

Supplemental Data

The following supplemental materials are available.

Supplemental Table S1. List of primers used in this study.

Supplemental Figure S1. In silico analysis of *MTP8* expression in Arabidopsis organs and in developing seeds.

Supplemental Figure S2. Concentrations of Fe, Mn, and Zn in seeds of Arabidopsis wild-type and *mtp8-1* and *vit1-2* single and *mtp8-1 vit1-2* double mutant lines.

Supplemental Figure S3. Effect of Mn availability on the germination of wild-type and *mtp8-1* seeds.

Supplemental Figure S4. Time-dependent Mn accumulation in seeds imbibed at increasing concentrations of Mn.

ACKNOWLEDGMENTS

We thank Lisa Gruber, Elis Fraust, Yudelsy Tandron-Moya, and Viviane Ott for excellent technical assistance and Mary-Lou Guerinot (Dartmouth College) for providing *vit1-1* mutant and *promoterVIT1-GUS* seeds.

Received October 28, 2016; accepted April 26, 2017; published May 1, 2017.

LITERATURE CITED

Arrivault S, Senger T, Krämer U (2006) The Arabidopsis metal tolerance protein AtMTP3 maintains metal homeostasis by mediating Zn exclusion from the shoot under Fe deficiency and Zn oversupply. Plant J **46:** 861–879

Bewley JD (1997) Seed germination and dormancy. Plant Cell **9:** 1055–1066

Borisjuk L, Nguyen TH, Neuberger T, Rutten T, Tschiersch H, Claus B, Feussner I, Webb AG, Jakob P, Weber H, et al (2005) Gradients of lipid storage, photosynthesis and plastid differentiation in developing soybean seeds. New Phytol **167:** 761–776

Bouis HE, Hotz C, McClafferty B, Meenakshi JV, Pfeiffer WH (2011) Biofortification: a new tool to reduce micronutrient malnutrition. Food Nutr Bull (Suppl) **32:** S31–S40

Bruch EM, Thomine S, Tabares LC, Un S (2015) Variations in Mn(II) speciation among organisms: what makes *D. radiodurans* different. Metallomics **7:** 136–144

Cailliatte R, Schikora A, Briat J-F, Mari S, Curie C (2010) High-affinity manganese uptake by the metal transporter NRAMP1 is essential for Arabidopsis growth in low manganese conditions. Plant Cell **22:** 904–917

Chen Z, Fujii Y, Yamaji N, Masuda S, Takemoto Y, Kamiya T, Yusuyin Y, Iwasaki K, Kato S, Maeshima M, et al (2013) Mn tolerance in rice is mediated by MTP8.1, a member of the cation diffusion facilitator family. J Exp Bot **64:** 4375–4387

Colangelo EP, Guerinot ML (2004) The essential basic helix-loop-helix protein FIT1 is required for the iron deficiency response. Plant Cell **16:** 3400–3412

Crosbie J, Longnecker N, Davies F, Robson A (1993). Effects of seed manganese concentration on lupin emergence. *In* J Barrow, ed, Plant Nutrition—from Genetic Engineering to Field Practice. Springer Dordrecht, The Netherlands, pp 665–668.

Curie C, Alonso JM, Le Jean M, Ecker JR, Briat JF (2000) Involvement of NRAMP1 from *Arabidopsis thaliana* in iron transport. Biochem J **347:** 749–755

Curie C, Cassin G, Couch D, Divol F, Higuchi K, Le Jean M, Misson J, Schikora A, Czernic P, Mari S (2009) Metal movement within the plant: contribution of nicotianamine and yellow stripe 1-like transporters. Ann Bot (Lond) **103:** 1–11

Delhaize E, Kataoka T, Hebb DM, White RG, Ryan PR (2003) Genes encoding proteins of the cation diffusion facilitator family that confer manganese tolerance. Plant Cell **15:** 1131–1142

Divol F, Couch D, Conéjéro G, Roschzttardtz H, Mari S, Curie C (2013) The Arabidopsis YELLOW STRIPE LIKE4 and 6 transporters control iron release from the chloroplast. Plant Cell **25:** 1040–1055

Donner E, Punshon T, Guerinot ML, Lombi E (2012) Functional characterisation of metal(loid) processes in planta through the integration of synchrotron techniques and plant molecular biology. Anal Bioanal Chem **402:** 3287–3298

Eggert K, von Wirén N (2013) Dynamics and partitioning of the ionome in seeds and germinating seedlings of winter oilseed rape. Metallomics **5:** 1316–1325

Eggert K, von Wirén N (2015) The role of boron nutrition in seed vigour of oilseed rape (*Brassica napus* L.). Plant Soil **402:** 63–76

Elble R (1992) A simple and efficient procedure for transformation of yeasts. BioTechniques **13:** 18–20

Eroglu S, Meier B, von Wirén N, Peiter E (2016) The vacuolar manganese transporter MTP8 determines tolerance to iron deficiency-induced chlorosis in Arabidopsis. Plant Physiol **170:** 1030–1045

Gilmour JT (1977) Micronutrient status of the rice plant. I. Plant and soil solution concentrations as a function of time. Plant Soil **46:** 549–557

Hokura A, Omuma R, Terada Y, Kitajima N, Abe T, Saito H, Yoshida S, Nakai I (2006) Arsenic distribution and speciation in an arsenic hyperaccumulator fern by X-ray spectrometry utilizing a synchrotron radiation source. J Anal At Spectrom **21:** 321–328

Hunter PR, Craddock CP, Di Benedetto S, Roberts LM, Frigerio L (2007) Fluorescent reporter proteins for the tonoplast and the vacuolar lumen identify a single vacuolar compartment in Arabidopsis cells. Plant Physiol **145:** 1371–1382

Kamijo N, Suzuki Y, Takano H, Tamura S, Yasumoto M, Takeuchi A, Awaji M (2003) Microbeam of 100 keV x-ray with a sputtered-sliced Fresnel zone plate. Rev Sci Instrum **74:** 5101–5104

Kim SA, Punshon T, Lanzirotti A, Li L, Alonso JM, Ecker JR, Kaplan J, Guerinot ML (2006) Localization of iron in Arabidopsis seed requires the vacuolar membrane transporter VIT1. Science **314:** 1295–1298

Lanquar V, Lelièvre F, Bolte S, Hamès C, Alcon C, Neumann D, Vansuyt G, Curie C, Schröder A, Krämer U, et al (2005) Mobilization of vacuolar iron by AtNRAMP3 and AtNRAMP4 is essential for seed germination on low iron. EMBO J **24:** 4041–4051

Lanquar V, Ramos MS, Lelièvre F, Barbier-Brygoo H, Krieger-Liszkay A, Krämer U, Thomine S (2010) Export of vacuolar manganese by AtNRAMP3 and AtNRAMP4 is required for optimal photosynthesis and growth under manganese deficiency. Plant Physiol **152:** 1986–1999

Li L, Chen OS, McVey Ward D, Kaplan J (2001) CCC1 is a transporter that mediates vacuolar iron storage in yeast. J Biol Chem **276:** 29515–29519

Martin MV, Fiol DF, Sundaresan V, Zabaleta EJ, Pagnussat GC (2013) oiwa, a female gametophytic mutant impaired in a mitochondrial

manganese-superoxide dismutase, reveals crucial roles for reactive oxygen species during embryo sac development and fertilization in Arabidopsis. Plant Cell **25:** 1573–1591

Mary V, Schnell Ramos M, Gillet C, Socha AL, Giraudat J, Agorio A, Merlot S, Clairet C, Kim SA, Punshon T, et al (2015) Bypassing iron storage in endodermal vacuoles rescues the iron mobilization defect in the natural resistance associated-macrophage protein3natural resistance associated-macrophage protein4 double mutant. Plant Physiol **169:** 748–759

Meguro R, Asano Y, Odagiri S, Li C, Iwatsuki H, Shoumura K (2007) Nonheme-iron histochemistry for light and electron microscopy: a historical, theoretical and technical review. Arch Histol Cytol **70:** 1–19

Migeon A, Blaudez D, Wilkins O, Montanini B, Campbell MM, Richaud P, Thomine S, Chalot M (2010) Genome-wide analysis of plant metal transporters, with an emphasis on poplar. Cell Mol Life Sci **67:** 3763–3784

Minet M, Dufour M-E, Lacroute F (1992) Complementation of Saccharomyces cerevisiae auxotrophic mutants by Arabidopsis thaliana cDNAs. Plant J **2:** 417–422

Montanini B, Blaudez D, Jeandroz S, Sanders D, Chalot M (2007) Phylogenetic and functional analysis of the Cation Diffusion Facilitator (CDF) family: improved signature and prediction of substrate specificity. BMC Genomics **8:** 107

Olsen LI, Hansen TH, Larue C, Østerberg JT, Hoffmann RD, Liesche J, Krämer U, Surblé S, Cadarsi S, Samson VA, et al (2016) Mother-plant-mediated pumping of zinc into the developing seed. Nat Plants **2:** 16036

Otegui MS, Capp R, Staehelin LA (2002) Developing seeds of Arabidopsis store different minerals in two types of vacuoles and in the endoplasmic reticulum. Plant Cell **14:** 1311–1327

Pedas P, Schiller Stokholm M, Hegelund JN, Ladegård AH, Schjoerring JK, Husted S (2014) Golgi localized barley MTP8 proteins facilitate Mn transport. PLoS One **9:** e113759

Peiter E, Fischer M, Sidaway K, Roberts SK, Sanders D (2005) The *Saccharomyces cerevisiae* Ca2+ channel Cch1pMid1p is essential for tolerance to cold stress and iron toxicity. FEBS Lett **579:** 5697–5703

Peiter E, Montanini B, Gobert A, Pedas P, Husted S, Maathuis FJM, Blaudez D, Chalot M, Sanders D (2007) A secretory pathway-localized cation diffusion facilitator confers plant manganese tolerance. Proc Natl Acad Sci USA **104:** 8532–8537

Pfaffl MW (2001) A new mathematical model for relative quantification in real-time RT-PCR. Nucleic Acids Res **29:** e45

Porter GS, Bajita-Locke JB, Hue NV, Strand D (2004) Manganese solubility and phytotoxicity affected by soil moisture, oxygen levels, and green manure additions. Commun Soil Sci Plant Anal **35:** 99–116

Punshon T, Hirschi K, Yang J, Lanzirotti A, Lai B, Guerinot ML (2012) The role of CAX1 and CAX3 in elemental distribution and abundance in Arabidopsis seed. Plant Physiol **158:** 352–362

Punshon T, Ricachenevsky FK, Hindt MN, Socha AL, Zuber H (2013) Methodological approaches for using synchrotron X-ray fluorescence (SXRF) imaging as a tool in ionomics: examples from *Arabidopsis thaliana*. Metallomics **5:** 1133–1145

Raboy V (2003) myo-Inositol-1,2,3,4,5,6-hexakisphosphate. Phytochemistry **64:** 1033–1043

Ricachenevsky FK, Menguer PK, Sperotto RA, Williams LE, Fett JP (2013) Roles of plant metal tolerance proteins (MTP) in metal storage and potential use in biofortification strategies. Front Plant Sci **4:** 144

Rodrigues-Filho UP, Vaz S Jr, Felicissimo MP, Scarpellini M, Cardoso DR, Vinhas RCJ, Landers R, Schneider JF, McGarvey BR, Andersen ML, et al (2005) Heterometallic manganese/zinc-phytate complex as a model compound for metal storage in wheat grains. J Inorg Biochem **99:** 1973–1982

Roschzttardtz H, Conéjéro G, Curie C, Mari S (2009) Identification of the endodermal vacuole as the iron storage compartment in the Arabidopsis embryo. Plant Physiol **151:** 1329–1338

Schaaf G, Honsbein A, Meda AR, Kirchner S, Wipf D, von Wirén N (2006) AtIREG2 encodes a tonoplast transport protein involved in iron-dependent nickel detoxification in *Arabidopsis thaliana* roots. J Biol Chem **281:** 25532–25540

Schnell Ramos M, Khodja H, Mary V, Thomine S (2013) Using μPIXE for quantitative mapping of metal concentration in *Arabidopsis thaliana* seeds. Front Plant Sci **4:** 168

Seregin IV, Kozhevnikova AD (2005) Distribution of cadmium, lead, nickel, and strontium in imbibing maize caryopses. Russ J Plant Physiol **52:** 565–569

Stacey MG, Patel A, McClain WE, Mathieu M, Remley M, Rogers EE, Gassmann W, Blevins DG, Stacey G (2008) The Arabidopsis AtOPT3 protein functions in metal homeostasis and movement of iron to developing seeds. Plant Physiol **146:** 589–601

Stadler R, Lauterbach C, Sauer N (2005) Cell-to-cell movement of green fluorescent protein reveals post-phloem transport in the outer integument and identifies symplastic domains in Arabidopsis seeds and embryos. Plant Physiol **139:** 701–712

Tegeder M (2014) Transporters involved in source to sink partitioning of amino acids and ureides: opportunities for crop improvement. J Exp Bot **65:** 1865–1878

Terada Y, Homma-Takeda S, Takeuchi A, Suzuki Y (2010) High-energy x-ray microprobe system with submicron resolution for x-ray fluorescence analysis of uranium in biological specimens. X-Ray Opt Instrum **2010:** 317909

Thomine S, Wang R, Ward JM, Crawford NM, Schroeder JI (2000) Cadmium and iron transport by members of a plant metal transporter family in Arabidopsis with homology to Nramp genes. Proc Natl Acad Sci USA **97:** 4991–4996

Thorne JH (1985) Phloem unloading of C and N assimilates in developing seeds. Annu Rev Plant Physiol **36:** 317–343

Vatansever R, Filiz E, Eroglu S (2017) Genome-wide exploration of metal tolerance protein (MTP) genes in common wheat (*Triticum aestivum*): insights into metal homeostasis and biofortification. Biometals **30:** 217–235

Weitbrecht K, Müller K, Leubner-Metzger G (2011) First off the mark: early seed germination. J Exp Bot **62:** 3289–3309

White PJ, Broadley MR (2009) Biofortification of crops with seven mineral elements often lacking in human diets–iron, zinc, copper, calcium, magnesium, selenium and iodine. New Phytol **182:** 49–84

Wierzbicka M, Obidzińska J (1998) The effect of lead on seed imbibition and germination in different plant species. Plant Sci **137:** 155–171

Wilson DO, Boswell FC, Ohki K, Parker MB, Shuman LM, Jellum MD (1982) Changes in soybean seed oil and protein as influenced by manganese nutrition. Crop Sci **22:** 948

Winzeler EA, Shoemaker DD, Astromoff A, Liang H, Anderson K, Andre B, Bangham R, Benito R, Boeke JD, Bussey H, Chu AM, et al (1999) Functional characterization of the S. cerevisiae genome by gene deletion and parallel analysis. Science **285:** 901–906